Received: 11 September 2020 | Revised: 1 December 2020 | Accepted: 26 December 2020

DOI: 10.1002/er.6408

RESEARCH ARTICLE

INTERNATIONAL JOURNAL OF ENERGY RESEARCH WILEY

Pressure-dependent elasto-mechanical stability and thermoelectric properties of $MYbF_3$ (M = Rb, Cs) materials for renewable energy

Rehan Ullah[1] | **Ali H. Reshak**[2,3,4] | **Malak Azmat Ali**[1] | **Afzal Khan**[5] | **Ghulam Murtaza**[6,7] | **Murefahmana AL-Anazy**[8] | **Hind Althib**[9,10] | **Tahani H. Flemban**[9,10]

[1]Department of Physics, Government Post Graduate Jahanzeb College Saidu Sharif, Swat, Pakistan

[2]Physics Department, College of Science, University of Basrah, Basrah, Iraq

[3]Faculty of Mechanical Engineering, Department of Instrumentation and Control Engineering, CTU in Prague, Technicka 4, Prague, Czech Republic

[4]Center of Excellence Geopolymer and Green Technology, School of Material Engineering, University Malaysia Perlis, Kangar, Malaysia

[5]Department of Physics, University of Peshawar, Peshawar, Pakistan

[6]Materials Modeling Lab, Department of Physics, Islamia College University, Peshawar, Pakistan

[7]Department of Mathematics & Natural sciences, Prince Mohammad Bin Fahd University, Alkhobar, Saudi Arabia

[8]Department of Chemistry, College of Science, Princess Nourah Bint Abdulrahman University, Riyadh, Saudi Arabia

[9]Basic and Applied Scientific Research Center, Imam Abdulrahman Bin Faisal University, Dammam, Saudi Arabia

[10]Department of Physics, College of Science, Imam Abdulrahman Bin Faisal University, Dammam, Saudi Arabia

Correspondence
Ali H. Reshak, Physics Department, College of Science, University of Basrah, Basrah, Iraq.
Email: maalidph@yahoo.co.uk

Summary

Pressure-dependent elasto-mechanical, thermoelectric and thermodynamic properties of two direct band gap halide perovskites $MYbF_3$ (M = Rb, Cs) have been investigated using density functional theory calculations. These calculations were carried out within Wein2k simulation code aided by generalized gradient approximation, Charpin method, BoltzTrap package and quasi-harmonic Debye model. The computed elastic constants (C_{11}, C_{12} and C_{44}) are all positive and follow the mechanical stability criteria within the applied pressure range (0-15 GPa). The obtained mechanical properties show that both the compounds are stiffer and oppose changes in the shape and volume up to a great extent. Moreover, $MYbF_3$ compounds are ductile and bonded with central forces whereas exhibiting unique properties in different crystallographic positions as shown by Zener anisotropic factor values. Thermoelectric parameters in the temperature range 200 to 800 K suggest these compounds for commercial thermoelectric device engineering due to low thermal conductivity, high electronic conductivity and moderate values of the figure of merit. The overall effect of thermodynamic parameters shows these compounds can withstand high temperature and pressure. The calculations specified these materials ideal for renewable energy generation.

KEYWORDS

density functional theory, elasto-mechanical, quasi-harmonic Debye model, thermodynamic parameters, thermoelectric parameters

1 | INTRODUCTION

Developing advanced, cost-effective and non-hazardous materials for practical use in renewable energy devices is an active area of research around the globe.[1,2] Generation of renewable energy needs innovative and tunable properties in materials for use in high-efficiency optoelectronic and thermoelectric devices. Halide perovskites are well-known in such perspective.[3-7] ABX_3 represents this class of materials where A cation is taken from alkali or alkaline earth metals, B cation from transition or post-transition or non-transition metals whereas X anion is taken from halogen.[8,9] Ideally, they crystallize in cubic forms in which A cation is 9- to 12-fold coordinated by X ion while B cation is sixfold coordinated by surrounding X ions. These materials exhibit fascinating properties such as ferroelectricity,[10] semiconductance,[11] superconductivity,[12] catalytic activity,[13] ionic conductivity[14] and thermoelectricity.[15] Moreover, their band gap values mostly fall in the infrared and visible range of electromagnetic radiation so they have motivated researchers for their use in renewable energy devices. Furthermore, they have the additional advantage of tunable physical properties with pressure and temperature.[16-18] On the basis of such characteristics, they have potential applications in vast areas of technology like multiferroic devices, solid oxide fuel cells, high Curie temperature superconductor,[19,20] energy domains, sensors, optoelectronics and field-effect transistors.[21-23]

Various attempts have been made both experimentally and theoretically for the investigation of halide perovskites in the last decade.[24] Two crucial members of halide perovskites are cesium- and rubidium-based fluoro-perovskites viz; $RbYbF_3$ and $CsYbF_3$. Their structural properties were experimentally and analytically explored elsewhere,[25-30] while a detailed first principle study on structural, electronic and optical properties under pressure was reported recently by Ullah et al[31] and Ali et al.[32] These studies show that $MYbF_3$ (M = Rb, Cs) compounds have perfect cubic geometry as well as direct band gap, falling in the visible limit of electromagnetic radiation. Therefore, they are much suitable for optoelectronic applications. Moreover, their tunable properties with the applied pressure make them a perfect material for pressure sensors. Though various physical properties of these compounds for vast applications have been studied, their elasto-mechanical and thermal properties are still unexplored. Although, one can deduce their optoelectronic functionalities but not their stability under high physical stress and high temperature. We, therefore, report the elasto-mechanical, thermoelectric and thermodynamic properties of $MYbF_3$ (M = Rb, Cs) investigated under pressure by first-principles density functional theory (DFT) calculations via FP-LAPW technique taking Wu-Cohen generalized gradient approximation (GGA)[33] as exchange-correlation potential. It has been found that this halide perovskite tolerates high mechanical stress and high temperature and are suitable for thermoelectric device applications.

2 | COMPUTATIONAL DETAILS

The optimized structural parameters are taken from our recent work[31,32] employed in the wein2k code.[34] Using the optimized structure, three elastic constants for cubic $MYbF_3$were computed through the density functional theory-based Charpin method.[35] A dense mesh of 1000k points was taken in the first Brillouin zone. Modified Beck-Johnson potential Equation (1)[36] along with GGA of Wu-Cohen[33] was implemented for self-consistent filed for evaluating thermoelectric and thermodynamic properties.

$$U_{x,\sigma}^{\mathrm{MBJ}}(\vec{r}) = CU_{x,\sigma}^{\mathrm{BR}}(\vec{r}) + (3C-2)\frac{1}{\pi}\sqrt{\frac{5}{12}}\sqrt{\frac{2t_\sigma(\vec{r})}{\rho_\sigma(\vec{r})}} \quad (1)$$

where $CU_{x,\sigma}^{\mathrm{BR}}\left(\vec{r}\right)$ is the Beck-Russel potential,[37] t_σ is the kinetic energy density and ρ_σ is the electronic density given by

$$\rho_\sigma = \frac{1}{2}\sum_{i=1}^{\sigma}\left|\psi_{i,\sigma}\right|^2 \quad (2)$$

We have implemented BoltzTraP (Boltzmann transport properties) code[38] for thermoelectric properties whereas the thermodynamic parameters were investigated via quasi-harmonic Debye model,[39] where the non-equilibrium Gibbs function $G^*(V, P, T)$ is given by

$$G(V;P;T) = E(V) + PV + A_{\mathrm{vib}}(\Theta(V);T) \quad (3)$$

where $E(V)$ and PV are unit cell energy and hydrostatic pressure condition, respectively. A_{vib} is the vibrational Helmholtz free energy while $\Theta_D(V)$ represents Debye temperature. The equilibrium state is obtained by minimizing G^* with respect to V.

3 | RESULTS AND DISCUSSION

3.1 | Elastic and mechanical results

Elastic properties explain the deformation in a compound under external pressure. Pressure alters the mechanical properties such as stiffness, stability and even the phase structure of a material. Therefore, it is very important to know the mechanical behavior of a compound before it is

used in device fabrication. Mechanical properties explain the possible micro-cracks in a compound during the growth process and suggest its suitability for industrial applications.[40] Three elastic constants: C_{11}, C_{12} and C_{44} are used to evaluate the elastic properties of cubic materials[41] and are given by the following relations.[42]

$$C_{11} = 4.133T\alpha B_T + \frac{e^2}{4r^4}[A_1/6 - 1.733B_1 + A_2/2 - 2.0666B_2] \quad (4)$$

$$C_{12} = 3.066T\alpha B_T + \frac{e^2}{4r^4}[A_1/6 - 1.3666B_1 + A_2/2 - 1.5333B_2] \quad (5)$$

$$C_{44} = -2.0666T\alpha B_T + \frac{e^2}{4r^4}[A_1/6 - 1.3666B_1 + A_2/2 - 1.5333B_2] \quad (6)$$

where,

$$T\alpha B_T = \frac{e^2}{4r^4}\left[0.3392\varepsilon^2 + B_1 - B_2\right] \quad (7)$$

The terms A_1, A_2, B_1 and B_2 are the short-range parameters as defined elsewhere[42] and α represents thermal expansion[43] and B_T is the isothermal bulk modulus. C_{11} elucidates the axis elasticity of the unit cell, C_{12} is the transverse expansion resistance and C_{44} is the shear deformation resistance, the latter two describe elasticity in the shape caused by transverse strain in the structure.[44] The idea of these elastic constants is presented pictographically in Figure 1. Table 1 shows that the C_{11}, C_{12} and C_{44} are all positive and follow the general criteria of mechanical stability,[42] that is, $(C_{11}\text{-}C_{12}) > 0$, $(C_{11} + 2C_{12}) > 0$ and $C_{44} > 0$. These constants are depicted as shown in Figure 2. The applied pressure (0-15 GPa) increased the values of elastic parameter (Table 1), the reason behind is the increase in density with the reduction of unit cell volume.

Furthermore, the computed elastic parameters were used to calculate other mechanical properties such as bulk modulus (B), shear modulus (G), Young modulus (E), Poisson ratio (ν), Pugh's ratio (B/G), Cauchy pressure (CP) and anisotropy (A) with the help of Equations (8) to (15).[45]

$$B = \frac{C_{11} + 2C_{12}}{3} \quad (8)$$

$$G = \frac{G_V + G_R}{2} \quad (9)$$

$$G_V = 1/5(C_{11} - C_{12} + 3C_{44}) \quad (10)$$

$$G_R = \frac{5C_{44}(C_{11} - C_{12})}{4C_{44} + 3(C_{11} - C_{12})} \quad (11)$$

$$E = \frac{9GB}{3B + G} \quad (12)$$

$$\nu = \frac{3B - 2G}{2(3B + G)} \quad (13)$$

$$CP = C_{12} - C_{44} \quad (14)$$

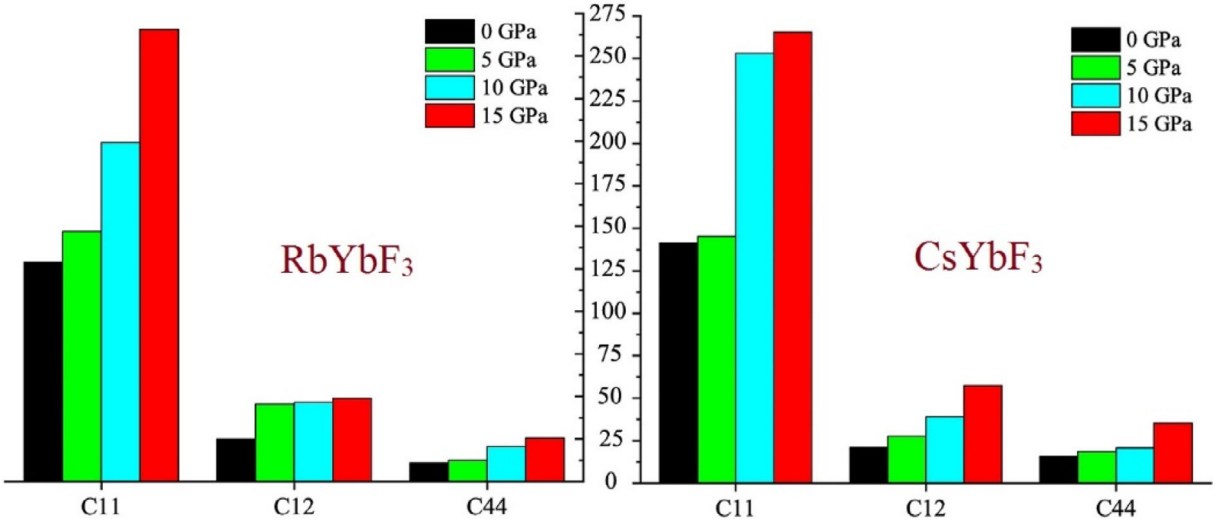

FIGURE 1 Cubic elastic constants representation as a derivative from stress and strain relations [Colour figure can be viewed at wileyonlinelibrary.com]

TABLE 1 Computed values of elastic and mechanical parameters of $MYbF_3$ (M = Rb, Cs)

	C_{11} (GPa)	C_{12} (GPa)	C_{44} (GPa)	B (GPa)	G (GPa)	E (GPa)	υ	B/G	C_{12}-C_{44}	A
$RbYbF_3$										
0 GPa	128.89	24.88	10.89	59.55	21.63	57.88	0.33	2.75	13.99	0.20
5 GPa	146.96	45.57	12.49	79.36	22.82	62.48	0.36	3.47	33.08	0.24
10 GPa	199.11	46.52	20.51	97.38	35.90	95.92	0.33	2.71	26.01	0.26
15 GPa	265.56	48.84	25.57	121.08	47.75	126.61	0.32	2.53	23.27	0.23
$CsYbF_3$										
0 GPa	141.19	20.95	15.66	61.03	27.84	72.49	0.30	2.19	5.29	0.26
5 GPa	145.21	27.59	18.53	66.79	30.08	78.46	0.30	2.22	9.06	0.31
10 GPa	253.03	39.06	20.72	110.38	42.90	113.95	0.32	2.57	18.34	0.19
15 GPa	265.55	57.42	35.38	126.8	55.46	145.21	0.30	2.28	22.04	0.33

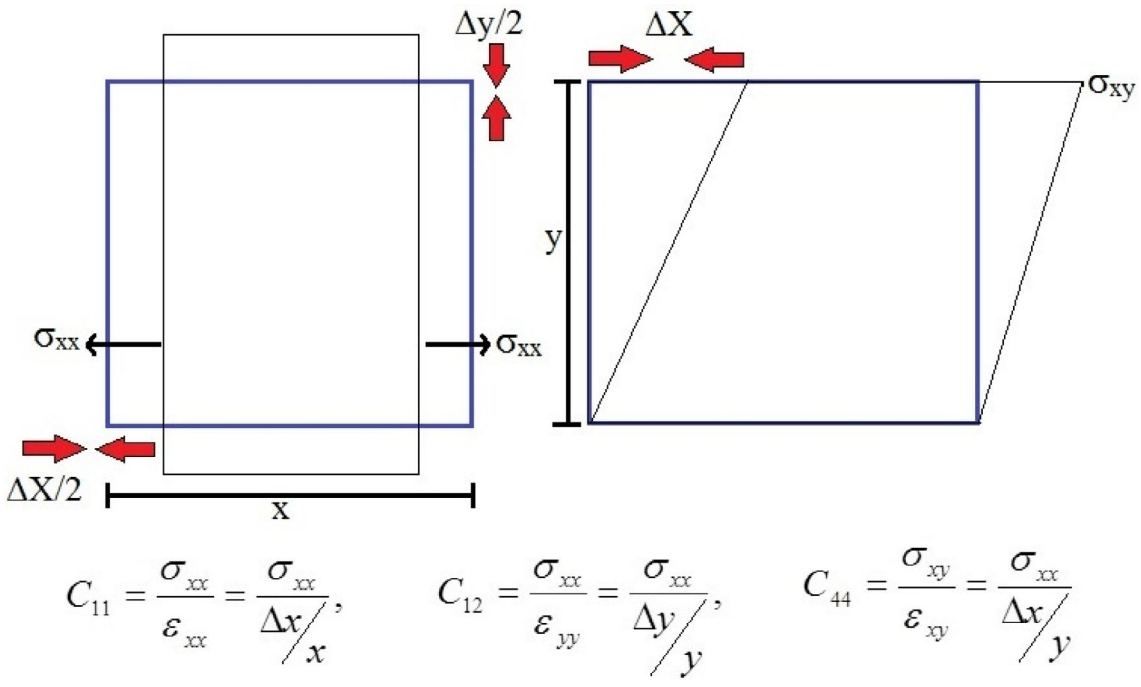

FIGURE 2 Pictographic representation of C_{11}, C_{12} and C_{44} for $MYbF_3$ (M = Rb, Cs) [Colour figure can be viewed at wileyonlinelibrary.com]

$$A = \frac{2C_{44}}{C_{11} - C_{12}} \tag{15}$$

B, *G* and *E*, respectively, represents the opposition of the material to change in volume, withstanding change in shape and the stiffness of the material. All the calculated values along with the elastic constants are given in Table 1. There are no other experimental and theoretical results available in the literature for the elastic constants of $MYbF_3$, to compare our results with. However, these results may serve as a reference for mechanical properties calculations in the future.

The large values of *B* and *G* indicate the $MYbF_3$ compounds are hard and can withstand the change in volume and shape, while the *E* values represent the given compound are stiffer in nature. The calculated values are observed to increase when pressure is applied. These characteristics favor the use of these compounds for mechanical applications where hard and stiffer materials are the priority.

The nature of bonding forces in $MYbF_3$ was examined using υ. For the central type forces, the ν should fall in the range from 0.25 to 0.5.[46] In case of $MYbF_3$, the bonding forces in $MYbF_3$ are central type as predicted by the

values of ν in Table 1. Ductility and brittleness categorize the materials for their industrial applications. The negative value of CP and value of B/G less than 1.75 shows brittle nature, while positive CP and B/G greater than 1.75 indicate ductility of materials.[46] From the data listed in Table 1, it is clear that at all the applied pressures, the B/G values are greater than 1.75 and CP values are all positive thereby showing the ductile nature of both compounds.

Whether a material is grown isotropic or anisotropic, this can be illustrated from the value of A, where its value is unity for isotropic behavior while deviation from it specifies the anisotropic nature of a compound. Our calculated values of A (Table 1) are all less than unity which shows the $MYbF_3$ are anisotropic compounds and will have different properties (like optical and mechanical) in different crystallographic directions. Moreover, the anisotropic nature remains the same even the pressure is increased to 15 GPa.

3.2 | Prospects of thermoelectric properties

In thermoelectric materials, the temperature gradient induces the charge carrier to move from high- to low-temperature regions.[47] This phenomenon is very useful in systems where the energy wastes in the form of heat. This waste heat can be converted back into electrical power by thermoelectric materials. As a reason, the $MYbF_3$ compounds are investigated for their thermoelectric properties for renewable energy resources. These properties can be enhanced by a number of techniques[48]; even a crystallographic change can tune a variety of thermoelectric behavior of a material.[47] Thermoelectric materials have a diverse range of practical applications in detectors, cooling systems and thermoelectric refrigerators.[49]

Perovskites materials are widely used for this purpose because of their low thermal conductivity and high electronic conductivity.[50] Moreover, a narrow band gap semiconductor can be used efficiently for thermoelectric purposes.[51,52] Therefore, in the present work, the pressure-dependent thermoelectric coefficients including carrier concentration (n), electrical conductivity (σ), electronic thermal conductivity (κ_e), lattice thermal conductivity (κ_l), Seebeck coefficient (S) and ground state (0 GPa) figure of merit (ZT) have been investigated via generalized semi-classical BoltzTraP package[38] integrated into the wein2k code. This package is based on rigid band approximation and standard Boltzmann kinetic transport theory. The pressure is varied from 0 to 15 GPa with a step size of 5 GPa. The relaxation time is taken to be a constant ($\tau = 10^{-14}$) whereas the temperature is varied from 200 to 800 K. The calculated plots of thermoelectric coefficients are shown in Figures 3A,B, 4A-F and 5G-J with corresponding values at 300 K at different pressures in Table 2.

Figure 3A,B shows the value of carrier concentration (n) at varied pressure and temperature. It can be seen that n has a direct while inverse relation with applied temperature and pressure, respectively. The values at 300 K at different pressures are given in Table 2.

Electrical conductivity σ, calculated for $MYbF_3$, is shown in Figure 4A,B. From Figure 4A,B, it can be seen that the values of electrical conductivity increase with the rise in temperature due to the thermal excitation of the electrons to the conduction band. Materials having high electrical conductivity are considered good for thermoelectric purposes because it overturns the Joule heating effect. From the plots, it is clear that σ is increasing with rise both in pressure and temperature, this trend remains

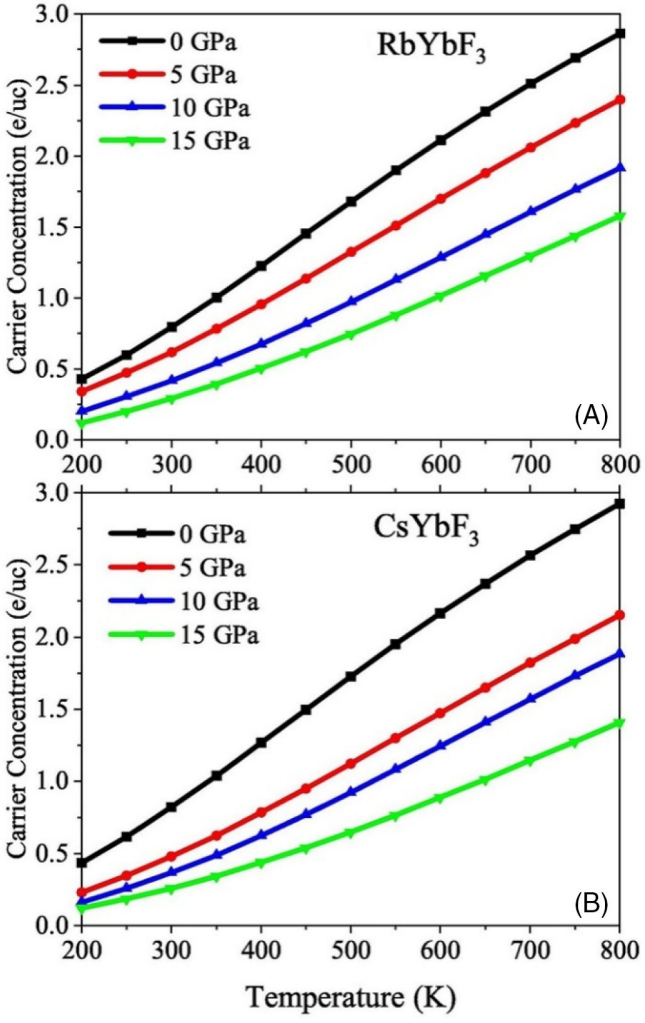

FIGURE 3 Temperature and pressure dependence of Carrier Concentration for, A, $RbYbF_3$, B, $CsYbF_3$ [Colour figure can be viewed at wileyonlinelibrary.com]

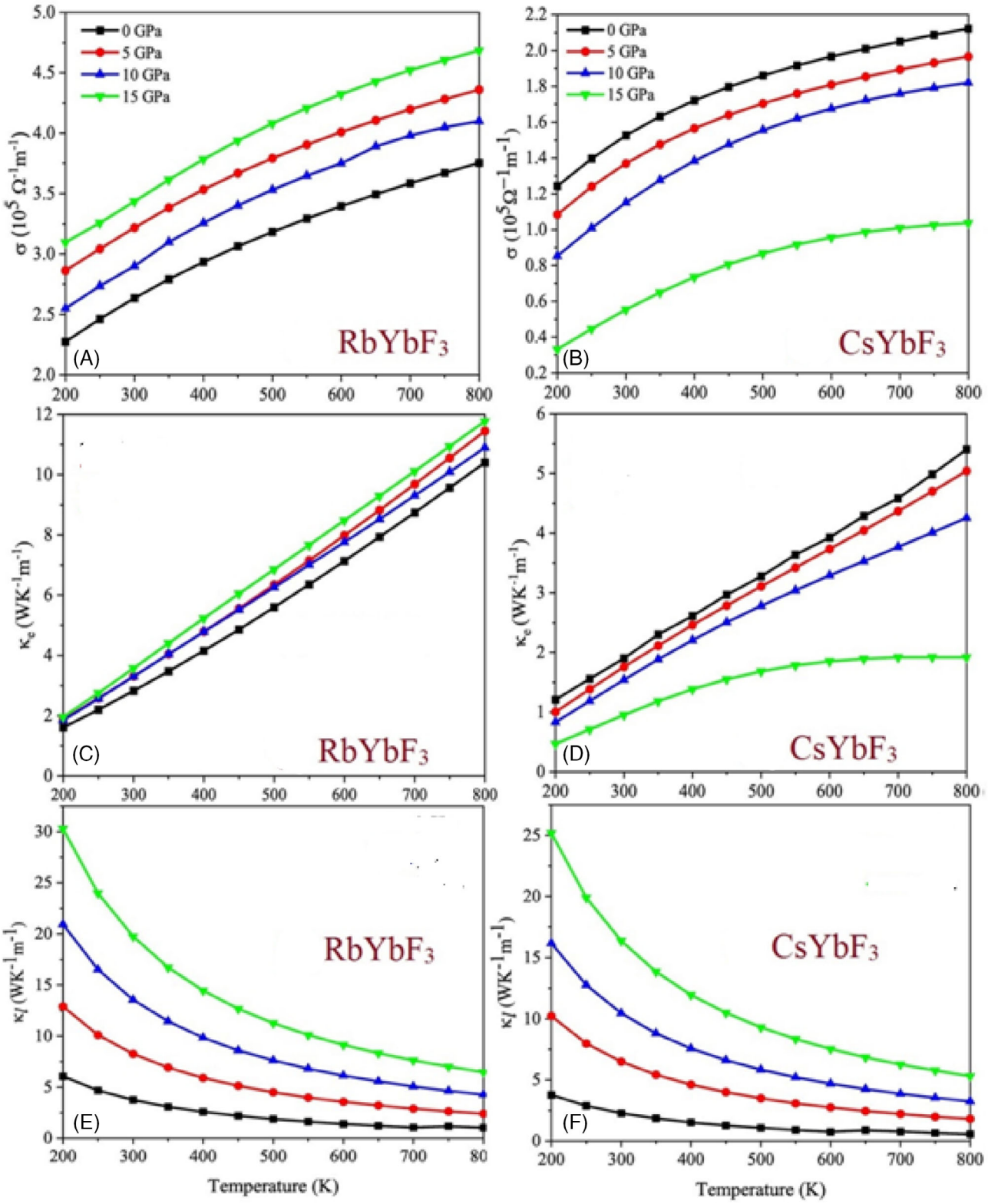

FIGURE 4 Temperature- and pressure-dependent curves of, A and B, electronic conductivity, C and D, electronic thermal conductivity, E and F, lattice thermal conductivity [Colour figure can be viewed at wileyonlinelibrary.com]

the same for temperature but becomes opposite for pressure when Rb is replaced with Cs cation. The high electrical conductivity (at 800 K) of $RbYbF_3$ is recorded as $3.75 \times 10^5\ \Omega^{-1}\ m^{-1}$ (0 GPa), $4.26 \times 10^5\ \Omega^{-1}\ m^{-1}$ (5 GPa), $4.36 \times 10^5\ \Omega^{-1}\ m^{-1}$ (10 GPa) and $4.68 \times 10^5\ \Omega^{-1}\ m^{-1}$ (15 GPa) whereas for $CsYbF_3$ it is calculated as

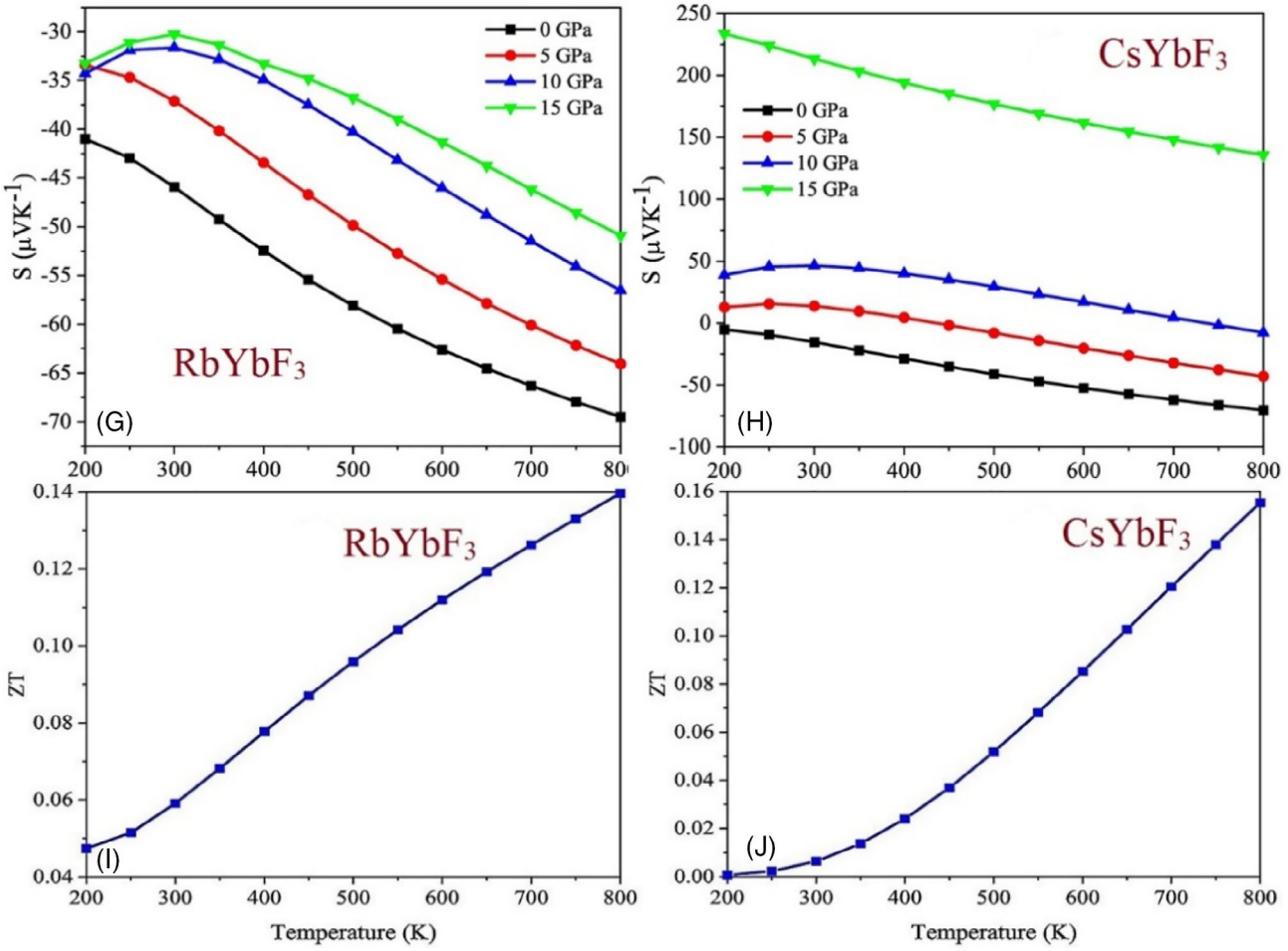

FIGURE 5 Temperature- and pressure-dependent curves of, G and H, Seebeck coefficient, I and J, Figure of merit [Colour figure can be viewed at wileyonlinelibrary.com]

TABLE 2 Computed values of thermoelectric parameters of $MYbF_3$ (M = Rb, Cs) at different pressures at 300 K

	n (e/uC)	σ $(\Omega\ m)^{-1}$	κe (W/mK)	κl (W/mK)	S (μV/K)	ZT
$RbYbF_3$						
P = 0 GPa	0.7942	2.64×10^5	2.83	3.75	−40.59	0.059
P = 5 GPa	0.6204	3.09×10^5	3.25	8.25	−30.71	0.039
P = 10 GPa	0.4162	3.22×10^5	3.30	13.55	−40.31	0.054
P = 15 GPa	0.2933	3.44×10^5	3.58	19.75	−30.22	0.030
$CsYbF_3$						
P = 0 GPa	0.2802	1.53×10^5	1.70	2.27	−10.54	0.006
P = 5 GPa	0.4789	1.42×10^5	1.76	6.48	10.38	0.004
P = 10 GPa	0.3651	1.15×10^5	1.54	10.45	40.64	0.048
P = 15 GPa	0.2581	0.553×10^5	0.95	16.38	200.14	0.079

$2.12 \times 10^5\ \Omega^{-1}\ m^{-1}$ (0 GPa), $2.10 \times 10^5\ \Omega^{-1}\ m^{-1}$ (5 GPa), $1.82 \times 10^5\ \Omega^{-1}\ m^{-1}$ (10 GPa) and $1.04 \times 10^5\ \Omega^{-1}\ m^{-1}$ (15 GPa). It is therefore concluded from Figure 4A,B that $RbYbF_3$ is a good electrical conductor as compared to $CsYbF_3$.

Another significant thermoelectric parameter is the thermal conductivity κ, which is the combined effect of electronic (κ_e) and lattice thermal conductivity (κl).[53] High thermal conductivity produces the heating effect in a material which results in high carrier resistance, therefore, for a

good thermoelectric material it should be low enough to achieve less carrier collision.[54,55] Electronic and lattice thermal conductivity calculated at different pressures for the $MYbF_3$ are shown in Figure 4C-F. For $RbYbF_3$ κ_e increases linearly with temperature for which the high values at 800 K are recorded as 10.4 W/Km (0 GPa), 11.3 W/Km (5 GPa), 11.4 W/Km (10 GPa) and 11.8 W/Km (15 GPa). For $CsYbF_3$ it also increases with temperature attaining the high values at 800 K as 5.41, 5.04, 4.26 and 1.92 W/Km at 0, 5, 10 and 15 GPa pressure, respectively. The applied pressure increases κ_e for $RbYbF_3$, while that for $CsYbF_3$ decreases. BoltzTrap only calculates the electronic contribution of thermal conductivity, therefore for the calculation of lattice thermal conductivity, we used Slack's Equation (16).[56]

$$\kappa_l = \frac{A\theta_D^3 V^{\frac{1}{3}} m}{\gamma^2 n^{\frac{2}{3}} T} \tag{16}$$

The required parameters (Debye temperature θ_D and Grüneisen parameter γ) were calculated through quasi-harmonic Debye approximation.[57] The resulted graphs at different pressures are depicted in Figure 4E,F. For both the compounds it has an inverse relation with temperature but direct relation with applied pressure. The values at different pressure and 300 K temperature are given in Table 2.

The conversion efficiency of thermoelectric materials is generally expressed in terms of Seebeck coefficient or thermopower (S). It can be calculated as the ratio of difference of voltage to the difference of temperature across the materials ($S = \Delta V/\Delta T$).[58,59] Moreover, taking this difference of potential with respect to temperature at zero current density also predicts Seebeck coefficient given by the relation.[50]

$$J = -\sigma\Delta V - \sigma S\Delta T \tag{17}$$

where J, ΔV and ΔT are sequentially represented current density, potential difference and temperature difference. At zero current density ($J = 0$), the differential form of S becomes $\Delta V = S\Delta T$.

The calculated plots of S for $MYbF_3$ compound are presented in Figure 5G,H. From the plots, it is clear that the value of S is decreasing as the temperature rises. The application of pressure tends the S to be increasing in the whole temperature region. Maximum observed ground state value in case of $RbYbF_3$ at 800 K temperature is −69.5 μV/K, this value reduces to −70.3 μV/K when Rb is replaced by Cs. Values of the Seebeck coefficients at room temperature and each applied pressure are tabulated in Table 2. Moreover, from Figure 5G and Table 2, it can be observed that the values of S in case of $RbYbF_3$ are all negative which reveals the n-type semiconducting behavior of $RbYbF_3$. At 0 GPa the $CsYbF_3$ also show the same behavior but at high pressure (5-15 GPa) the n-type changes to p-type behavior. Therefore, we can conclude negative charge as the majority charge carrier in the former compound, while in the latter compound the applied pressure enhances positive charge carriers over the negative. The inverse relation of electrical conductivity and Seebeck coefficient is the indication of good thermoelectrical behavior of these studied compounds.

The thermoelectric performance of the given materials is studied by plotting the figure of merit (ZT) at 0 GPa pressure. ZT can be derived from the product of the square of Seebeck coefficient and electrical conductivity divide by thermal conductivity. Here in our case, we have only taken electronic thermal conductivity for the ZT calculation. The ZT is made dimensionless by multiplying T with the obtained result.[60,61]

$$ZT = \frac{S^2\sigma}{\kappa_e} T \tag{18}$$

The calculated dimensionless ZT as a function of temperature is shown in Figure 5I,J. The ZT value increases in the whole temperature region. Its values at 800 K are 0.14 and 0.15 for $RbYbF_3$ and $CsYbF_3$, respectively. These low values are due to the low thermal conductivity and low carrier concentration. The values of ZT at different pressure values at room temperatures are given in Table 2.

This study of thermoelectric behaviors of $MYbF_3$ suggests that these compounds could be efficiently used for thermoelectric renewable energy generation on a commercial level.

3.3 | Thermodynamic properties

Thermodynamic properties comprising of Debye temperature (θ_D), Grüneisen parameter (γ), thermal expansion coefficient (α) and specific heat capacity (c_v) of $MYbF_3$ were extracted via employing the ground state structural parameters through quasi-harmonic Debye model.[62] The temperature (200-800 K) and pressure (0-15 GPa) varied results are as depicted in Figures 6A-D and 7E-H.

Debye temperature is used to figure out other important parameters such as melting temperature and specific heat capacity (Equation 20). Furthermore, it is related to phonon transfer speed (ν) by the relation[63]:

$$\theta_D = \frac{\hbar\nu}{K_B}\left(6\pi^2 N\right)^{\frac{1}{3}} \tag{19}$$

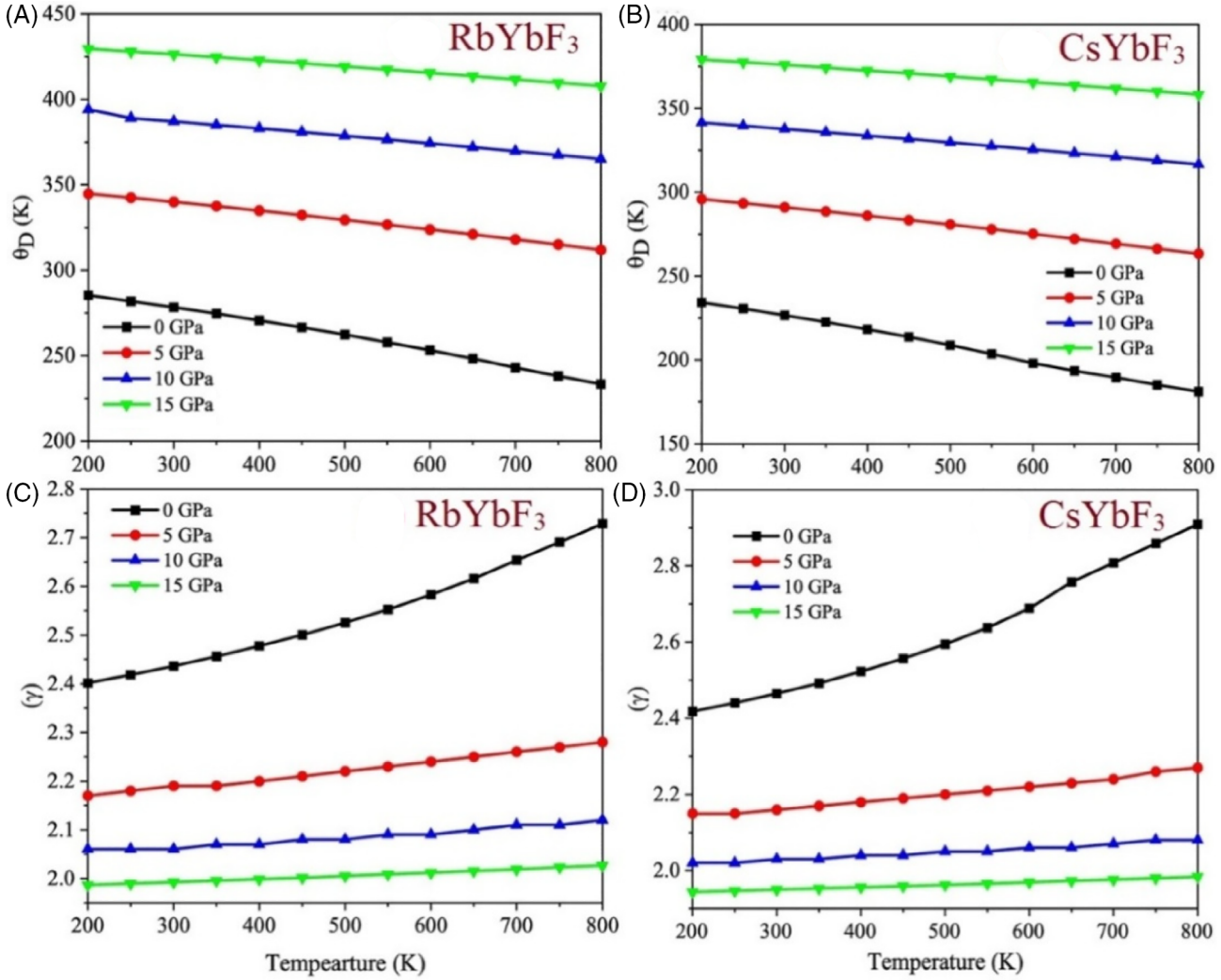

FIGURE 6 Computed plots of, A and B, Debye temperature, C and D, Grüneisen parameter at different pressure and temperatures [Colour figure can be viewed at wileyonlinelibrary.com]

where N represents the number of atoms per unit cell and k_B is the Boltzmann constant.[64]

At constant pressure, the Debye temperature decreases with the rise in temperature and follows an almost linear relationship, as shown in Figure 7A,B. On the other side, at a room temperature (300 K), it increases by 53.21% for $RbYbF_3$ while by 65.86% for $CsYbF_3$, when the external pressure rises from 0 to 15 GPa. The reported Debye temperatures at 0 GPa and 200 K are 285.34 K ($RbYbF_3$) and 234.24 K ($CsYbF_3$). As from Equation (19), the phonon transfer speed has a direct relation with Debye temperature, so at low temperatures, the phonon transfer speed of $RbYbF_3$ is heightened as compared to $CsYbF_3$. The values of 800 K temperature and varied pressures are given in Table 3.

The Grüneisen parameter (γ) provides information about the change in vibrational frequency in lattice with applied temperature and characterizes the thermo-elastic response of a compound.

Its values are calculated and plotted in Figure 6C,D. It is observed that γ slightly increases with varying temperatures at 0, 5 and 10 GPa pressures, while a significant increase is noticed at 15 GPa pressure. This increase with temperature suggests the involvement of phonon in lattice part of thermal conductivity. The calculated value of γ at 300 K temperature and 0 GPa pressure are 2.40 and 2.42 for $RbYbF_3$and $CsYbF_3$, respectively.

The specific heat capacity (c_v) is investigated to know the capability of studied compounds for tolerating the externally applied temperature. Dulong-Petit law and Einstein model explains c_v curve at high-temperature region but unable to explains the experimental relation $c_v \propto T^3$. In the low-temperature region, the in-phase atomic vibrations dominate acoustic phonons while in the high-temperature region, out phase atomic vibrations dominate optical phonons. The optical phonon mode could be easily explained by individual vibrations while acoustic phonon mode could be

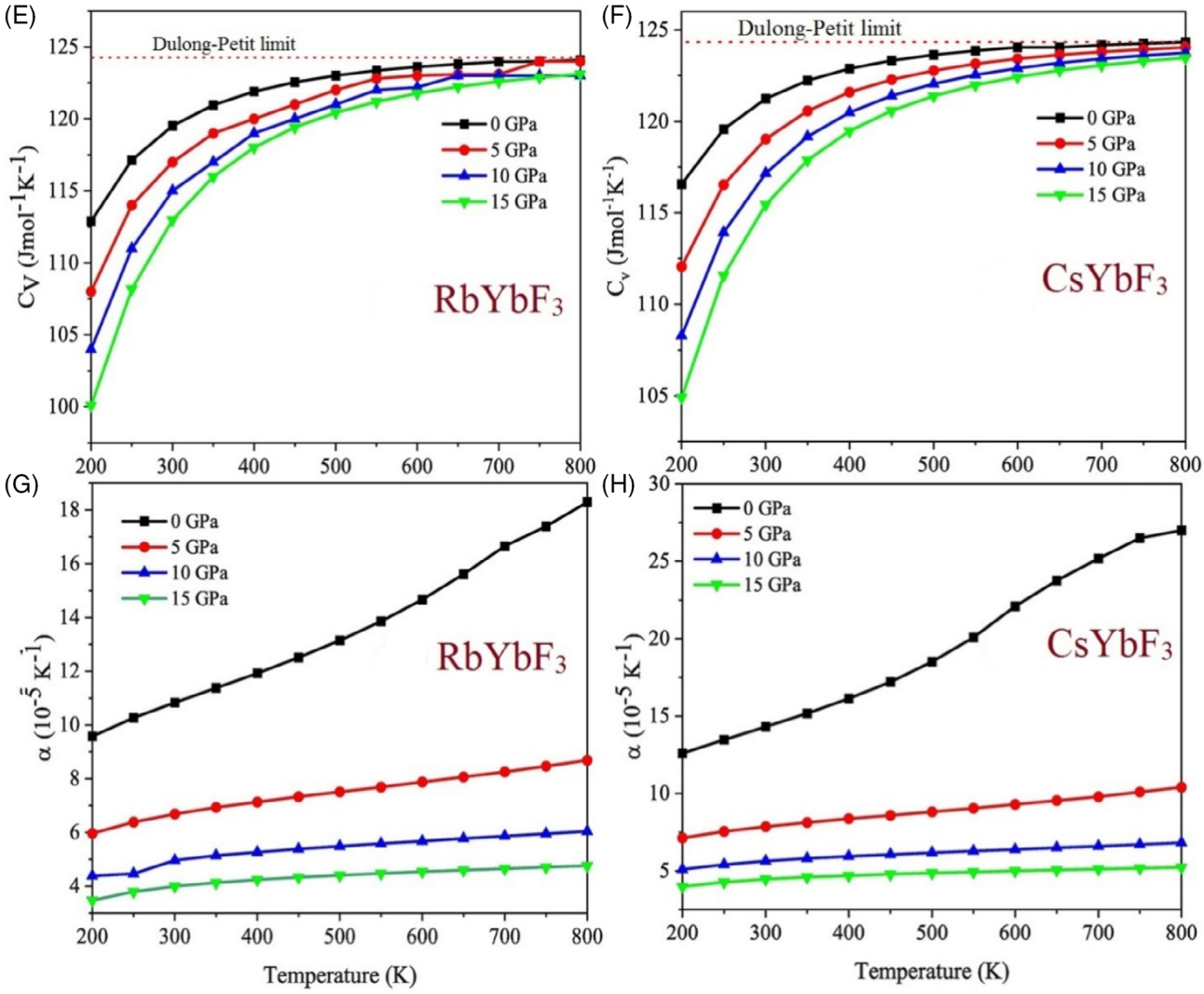

FIGURE 7 Computed plots of, E and F, specific heat capacity, G and H, volumetric thermal expansion at different pressures and temperatures [Colour figure can be viewed at wileyonlinelibrary.com]

TABLE 3 Thermodynamic values of $MYbF_3$ (M = Rb, Cs) at different pressures and high temperature (800 K)

	θ_D (K)	γ	C_V ($Jmol^{-1}\,K^{-1}$)	α (K^{-1})
$RbYbF_3$				
P = 0 GPa	240.36	2.60	124	18.2×10^{-5}
P = 5 GPa	311.97	2.28	124	8.69×10^{-5}
P = 10 GPa	365.15	2.12	123	6.05×10^{-5}
P = 15 GPa	407.8	2.02	123	4.77×10^{-5}
$CsYbF_3$				
P = 0 GPa	183.01	2.85	124	20.5×10^{-5}
P = 5 GPa	236.26	2.27	124	10.4×10^{-5}
P = 10 GPa	316.63	2.08	124	6.82×10^{-5}
P = 15 GPa	358.19	1.98	123	5.25×10^{-5}

explained without considering the vibrational interaction. Therefore, Debye solves the problem by considering that the atoms do not vibrate individually with the same frequency. These are coupled together with a large number of frequencies instead of a single frequency. The mathematical relation of C_v in-terms of Debye temperature can be written as

$$C_v = 9R\left(\frac{T}{\theta_D}\right)^3 \int_0^{Xm} \frac{x^4 e^x}{(e^x-1)^2} dx \quad (20)$$

where θD is the Debye temperature, R is the ideal gas constant and N is the number of atoms.[65] Our plotted results of c_v are depicted in Figure 7E,F against pressure and temperature, which clarify that both the compounds display an abrupt increase in c_v with the rise in temperature up to 550 K, behind 550 K, the slope gradually slows down and at higher temperatures, it becomes constant. This is consistent with the Dulong-Petit limit satisfied by the Debye model.[66] The values for c_v at 0 GPa and 800 K were computed to be 124.78 and 124.79 J mol^{-1} K for $RbYbF_3$ and $CsYbF_3$, respectively. The pressure application reduced the values of specific heat capacity. The specific heat capacity values (Table 3) shows the high potential of $MYbF_3$ to sustain external temperatures. Additionally, $CsYbF_3$ has relatively greater thermal stability as compared to $RbYbF_3$.

Figure 7G,H depicts the change in the volume the thermal expansion coefficient (α) with external pressure and temperature using the relation (21) as

$$\alpha = \frac{\gamma C_v}{B_T V} \quad (21)$$

Here, B_T, V and C_V are the isothermal bulk modulus, unit formula volume and specific heat at constant volume, respectively.

From the figures, we can state that the volume of these compounds expands as the temperature rises, this volumetric expansion is slightly observed at high pressures (10 and 15 GPa) while this effect is majorly perceived at low 0 GPa pressure. The values of α at different pressures and 800 K temperature are given in Table 3.

Due to the unavailability of any theoretical or experimental data, we could not compare our results. Still we hope, the present calculations can serve as reference data for future work regarding the thermodynamic properties of these perovskites.

4 | CONCLUSION

In this investigation, a broad study of pressure-dependent (0-15 GPa) elastic, mechanical, thermoelectric and thermodynamic properties of $MYbF_3$ (M = Rb, Cs) is carried out within highly precise DFT using FP-LPAW scheme programmed in Wein2k simulation code. The elastic constants are computed using Charpin method. The elastic constants are all positive and follow the stability criteria, therefore the given compounds are mechanically stable at all applied pressures. The mechanical behavior studied through bulk modulus, shear modulus, Young's modulus, and anisotropy factor reveals the stiffer, hard and anisotropic nature of the herein studied compounds. Moreover, allowed values of Poisson's ratio and Cauchy pressure disclose the compounds are ductile and have central forces between the constituent atoms. On the basis of mechanical properties, we believe that these compounds can resist any change in volume, shape and are mechanically stable in their respective device-based applications. Boltzmann theory and Slack's model are used for the calculation of thermoelectric properties. The pressure and temperature (200-800 K) reliant thermoelectric properties are calculated in terms of electronic conductivity, thermal conductivity (electronic and lattice), Seebeck coefficient and figure of merit. These parameters show changes with pressure which make these studied perovskites suitable for converting thermal energy into electrical energy due to their high electronic conductivity, low thermal conductivity and high conversion efficiency at low temperatures. Our calculated thermodynamic coefficients clarify that $MYbF_3$materials can work at high temperatures. Pressure inclusion reduced the values of Grüneisen parameter, specific heat capacity and volumetric thermal expansion while the increase is observed in Debye temperature. The values acquired in this work recommend the $MYbF_3$ for mechanical and thermo-electronic-based devices.

ACKNOWLEDGEMENT

Murefah mana AL-Anazy extended her sincere appreciation to the Deanship of Scientific Research at Princess Nourah Bint Abdulrahman University through the Fast-track Research Funding Program.

DATA AVAILABILITY STATEMENT

Data sharing not applicable to this article as no datasets were generated or analyzed during the current study (the article describes entirely theoretical research).

ORCID

Ali H. Reshak https://orcid.org/0000-0001-9426-8363
Malak Azmat Ali https://orcid.org/0000-0002-6290-0317
Ghulam Murtaza https://orcid.org/0000-0001-5520-2265

REFERENCES

1. Lukatskaya MR, Dunn B, Gogotsi Y. Multidimensional materials and device architectures for future hybrid energy storage. *Nat Commun*. 2016;7:12647.
2. Ye WN, Xiong Y. Review of silicon photonics: history and recent advances. *J Modern Optics*. 2013;60:16.

3. Noguera C. *Physics and Chemistry at Oxide Surfaces*. New York: Cambridge University Press; 1996.
4. Murtaza G, Ahmad I. First principle study of the structural and optoelectronic properties of cubic perovskites CsPbM3 (M=Cl, Br, I). *Phys B Condensed Matter*. 2011;406:3222-3229.
5. Murtaza G, Khenata R, Khalid MN, Naeem S. Elastic and opto-electronic properties of RbMF3 (M = Zn, Cd, Hg): A mBJ density functional calculation. *Phys B Condensed Matter*. 2013;410:31.
6. Agbaoye RO, Adebambo PO, Adebayo GA. First principles comparative studies of thermoelectric and other properties in the cubic and hexagonal structure of CsCdCl3 halide perovskites. *Comput Condensed Matter*. 2019;21:388.
7. Mubarak AA. Ab initio study of Ag-based Fluoroperovskite AgMF3 (M = Co and Ni) compounds. *J Electron Mater*. 2018; 47:887-898.
8. Erum N, Iqbal MA. First principles investigation of fluorine based strontium series of perovskites. *Commun Theor Phys*. 2016;66:571-578.
9. Murtaza G, Sadique G, Rahnamaye-Aliabad HA, et al. First principle study of cubic perovskites: AgTF3 (T = Mg, Zn). *Physica B*. 2011;406:4584-4589.
10. Bednorz JG, Muller KA. Sr1−xCaxTiO$_3$: AnXYQuantum ferroelectric with transition to randomness. *Phys Rev Lett*. 1984;52: 2289-2292.
11. Frederikse HPR, Thurber WR, Hosler WR. Electronic transport in strontium titanate. *Phys Rev*. 1964;134:A442-A445.
12. Koonce CS, Cohen ML, Schooley JF, Hosler WR, Pfeiffer ER. Superconducting transition temperatures of semiconducting SrTiO$_3$. *Phys Rev*. 1967;163:380-390.
13. Henrich VE. The surfaces of metal oxides. *Rep Prog Phys*. 1985; 48:1481-1541.
14. Kharton VV, Marques FMB, Atkinson A. Transport properties of solid oxide electrolyte ceramics: a brief review. *Solid State Ion*. 2004;174:135-149.
15. Muta H, Kurosaki K, Yamanaka S. Thermoelectric properties of rare earth doped SrTiO$_3$. *J Alloys Compd*. 2003;350:292-295.
16. Ramesh R, Spaklin NA. Multiferroics: progress and prospects in thin films. *Nature Mater*. 2007;6:21-29.
17. Scott JF. Nanoferroelectrics: statics and dynamics. *J Phys Condens Matter*. 2006;18:R361-R386.
18. Bokov AA, Ye ZG. Recent progress in relaxor ferroelectrics with perovskite structure. *J Mater Sci*. 2006;41:31-52.
19. Kao WH, Haberichter SL, Bullock KR. Corrosion resistant coating for a positive Lead/acid battery electrode. *J Electrochem Soc*. 1992;139:L105-L107.
20. Auciello O, Scott JF, Ramesh R. The physics of ferroelectric memories. *Phys Today*. 1998;51:22-27.
21. Murtaza G, Ahmad I, Amin B, et al. Investigation of structural and optoelectronic properties of BaThO3. *Opt Mater*. 2011; 33:553.
22. Kagan CR, Mitzi DB, Dimitrakopoulos CD. Organic-inorganic hybrid materials as semiconducting channels in thin-film field-effect transistors. *Science*. 1999;286:945-947.
23. Klauk H. Molecular electronics on the cheap. *Phys World*. 2000;13:18-19.
24. Dar SA, Srivastava V, Sakalle UK, Parey V, Pagare G. DFT investigation on electronic, magnetic, mechanical and thermodynamic properties under pressure of some EuMO3(M = Ga, In) perovskites. *Mater Res Express*. 2017;4:106104.
25. Moreira RL, Dias A. Comment on "prediction of lattice constant in cubic perovskites". *PhysChem Solids*. 2007;68:1617-1622.
26. Terki R, Feraoun H, Bertrand G, Aourag H. Full potential calculation of structural, elastic and electronic properties of BaZrO3 and SrZrO3. *Phys. Stat. Sol (b)*. 2005;242(5):1054-1062. https://dx.doi.org/10.1002/pssb.200402142.
27. Verma AS, Kumar AJ. Bulk modulus of cubic perovskites. *Alloys Compd*. 2012;541:210-214.
28. Jiang LQ, Guo JK, Liu HB, et al. Prediction of lattice constant in cubic perovskites. *Phys Chem Solids*. 2006;67:1531-1536.
29. Verma AS, Jindal VK. Lattice constant of cubic perovskites. *J Alloys Compd*. 2009;485:514-518.
30. Ubic R. Revised method for the prediction of lattice constants in cubic and pseudocubic perovskites. *J Am Ceram Soc*. 2007; 90:3326-3330.
31. Ullah R, Ali MA, Murad S, et al. Structural, electronic and optical properties of cubic perovskite RbYbF3under pressure: a first principles study. *Mater Res Exp*. 2019;6(2019):125901.
32. Ali MA, Ullah R, Murad S, et al. Insight into pressure tunable structural, electronic and optical properties of "equation missing" via DFT calculations. *The European Physical Journal Plus*. 2020;135:309.
33. Wu Z, Cohen RE. More accurate generalized gradient approximation for solids. *Phys Rev B*. 2006;73:235116.
34. Bhala P, Schwarz K, Madsen GKH, Kvanicka D, Luitz J. *WIEN2K, an Augmented Plane Wave Local Orbital Program for Calculating Crystal Properties Karlheinz Schwarz*. Wien: Technische Universitat; 2001.
35. Charpin T. A Package for Calculating Elastic Tensors of Cubic Phases Using WIEN: Laboratory of Geometrix F-75252 (Paris, France); 2001
36. Tran F, Blaha P. Accurate Band Gaps of Semiconductors and Insulators with a Semilocal Exchange-Correlation Potential. *Phys Rev Lett*. 2009;102(1):226401.
37. Becke AD, Roussel MR. Exchange holes in inhomogeneous systems: a coordinate-space model. *Phys Rev A*. 1989;39:3761-3767.
38. Madsen GK, Singh DJ. BoltzTraP. A code for calculating bandstructure dependent quantities. *Comput PhysCommun*. 2006;175(1):67-71.
39. Flórez M, Recio JM, Francisco E, Blanco MA, Pendás A M'n. First-principles study of the rocksalt–cesium chloride relative phase stability in alkali halides. *Phys Rev B*. 2002;66:144112.
40. Khandy SA, Yousuf S, Gupta DC. Structural, Magneto-electronic, Mechanical, and Thermophysical Properties of Double Perovskite Ba2ZnReO6. *Phys Status Solidi (B) Basic Res*. 2019; 256(10):1800625.
41. Parveen A, Gaur NK. Elastic and thermodynamic properties of AVO$_3$ (A = Sr, Pb) perovskites. *Phys B Condensed Matter*. 2012; 407:500-504.
42. Kaur N, Mohan R, Gaur NK, Singh RK. The elastic and thermodynamic properties of antiperovskites: MCNi$_3$. *J Alloys Compd*. 2010;491:284-290.
43. Belik AA, Azuma M, Saito T, Shimakawa Y, Takano M. Crystallographic features and tetragonal phase stability of PbVO$_3$, a new member of PbTiO3Family. *Chem Mater*. 2005;17:269-273.
44. Voigt W. *Lehrbuch der Kristallphysik*. Leipzig: B. B. Teubner; 1928:739.
45. Cherid S, Benstaali W, Abbad A, et al. Theoretical prediction of half metallic ferromagnetic full-Heusler alloys Cs$_2$CrGe. *SolidStateCommun*. 2017;260:14-18.
46. Ghosh S, Gupta DC. Electronic, magnetic, elastic and thermodynamic properties of Cu$_2$MnGa. *J Magn Magn Mater*. 2016; 411:120-127.

47. Mahmood Q, Ashraf A, Hassan M. Investigations of optical and thermoelectric response of direct band gap Ca3XO (X = Si, Ge) anti-perovskites stabilized in cubic and orthorhombic phases. *Indian J Phys*. 2018;92:86.
48. Amin B, Singh N, Tritt TM, Alshareef HN, Schwingenschlogl U. Major enhancement of the thermoelectric performance in Pr/Nb-doped SrTiO3 under strain. *Appl Phys Lett*. 2013;103:031907.
49. Noor NA, Hassan M, Rashid M, Alay-e-Abbas SM, Laref A. Systematic study of elastic, electronic, optical and thermoelectric properties of cubic $BiBO_3$ and $BiAlO_3$ compounds at different pressure by using ab-initio calculations. *Mater Res Bull*. 2018;97:436-443.
50. Noor NA, Mahmood Q, Rashid M, Ul Haq B, Laref A, Ahmad SA. Ab-initio study of thermodynamic stability, thermoelectric and optical properties of perovskites ATiO3 (A = Pb, Sn). *J Solid State Chem*. 2018;263:115-122.
51. Sun P, Oeschler N, Johnsen S, Iversen BB, Steglich F. Narrow band gap andenhanced thermoelectricity in $FeSb_2$. *Dalton Trans*. 2010;39(4):1012-1019.
52. Kim I-H. Mg2BIV: Narrow bandgap thermoelectric semiconductors. *J Korean Phys Soc*. 2018;72(10):1095-1109.
53. Hassan M, Arshad I, Mahmood Q. Computational Study of Electronic, Optical and Thermoelectric Properties of X3PbO (X = Ca, Sr, Ba) Anti-perovskites. *Semicond Sci Technol*. 2017;32:115002.
54. Slack GA. The Thermal Conductivity of Nonmetallic Crystals. *Solid St Phys*. 1979;34:1.
55. Zhao K, Qiu P, Shi X, Chen L. Recent Advances in Liquid-Like Thermoelectric Materials. *Adv Funct Mater*. 2020;30:1903867.
56. Xiao-Lei Shi JZ, Chen Z-G. Advanced Thermoelectric Design: From Materials and Structures to Devices. *Chem Rev*. 2020;120:7399-7515.
57. Francisco E, Blonco MA, Sanjurjo G. Atomistic simulation of SrF_2 polymorphs. *Phys Rev B*. 2001;63:049107.
58. Takeuchi T. Conditions of electronic structure to obtain large dimensionless figure of merit for developing practical thermoelectric materials. *Mater Trans*. 2009;50:2359-2365.
59. Khandy SA, Gupta DC. Structural, elastic and thermoelectronic properties of paramagnetic perovskite $PbTaO_3$. *RSC Adv*. 2016;6:48009-48015.
60. Riffat SB, Ma X. Thermoelectrics: a review of present and potential applications. *Appl Therm Eng*. 2003;23:913-935.
61. Bhamu KC, Soni A, Sahariya J. Revealing optoelectronic and transport properties of potential perovskites Cs2PdX6 (X = Cl, Br): a probe from density functional theory (DFT). *Solar Energy*. 2018;162:336-343.
62. Blanco MA, Francisco E, Luania V. Gibbs2: a new version of the quasi-harmonic model code. I. Robust treatment of the static data. *Comput Phys Commun*. 2004;158:57-72.
63. Zhang FP, Zhang X, Lu QM, Zhang JX, Liu YQ. Electronic structure and thermal properties of doped $CaMnO_3$ systems. *J Alloys Compd*. 2011;509:4171-4175.
64. Takahata K, Iguchi Y, Tanaka D, Itoh T, Terasaki I. Low thermal conductivity of the layered oxide (Na,Ca)Co2O4: Another example of a phonon glass and an electron crystal. *Phys Rev B*. 2000;61:12551.
65. Wahab MA. *Solid State Physics, Structure and Properties of Materials*. 2nd ed. Oxford, UK: Alpha Science International; 2005:596.
66. Petit AT, Dulong PL. Researches on the Measureof Temperatures, and on the Laws of the Communica-tion of Heat. *Ann Chim Phys*. 1819;10:395.

How to cite this article: Ullah R, Reshak AH, Ali MA, et al. Pressure-dependent elasto-mechanical stability and thermoelectric properties of $MYbF_3$ (M = Rb, Cs) materials for renewable energy. *Int J Energy Res*. 2021;1–13. https://doi.org/10.1002/er.6408